View Article Online
View Journal

Dalton Transactions

An international journal of inorganic chemistry

This article can be cited before page numbers have been issued, to do this please use: S. Wang, S. Li, R. Shi, X. Zou, Z. Zhang, G. Fu, L. Li and F. Luo, *Dalton Trans.*, 2020, DOI: 10.1039/C9DT04485J.

ROYAL SOCIETY OF CHEMISTRY

rsc.li/dalton

View Article Online
DOI: 10.1039/C9DT04485J

Nanohybrid Self-Assembled by Exfoliated Layered Vanadium Oxide Nanosheets with Keggin Al_{13} for Selective Catalytic Oxidation of Alcohols

Received 00th January 20xx,
Accepted 00th January 20xx

DOI: 10.1039/x0xx00000x

Shuang Wang,[a] Shuying Li, [a] Rui shi, [a] Xinyu Zou, [a] Zhijuan Zhang, [a] Guoyuan Fu, [a] Lei Li, [a] Fang Luo*, [a]

ABSTRACT: A nanoscale hybrid material (V_2O_5-Al_{13}) for highly efficient alcohol oxidation is synthesized through electrostatic self-assembly between oppositely charged Keggin Al_{13} polyoxocations and exfoliated V_2O_5 nanosheets. The analysis by X-ray diffraction, electron microscopy, X-ray photoelectron spectrum and structural consideration based on charge balance indicate that Keggin Al_{13} ions could be sparsely distributed in the nanosheet galleries. The as-prepared catalyst successfully achieved high catalytic activity toward alcohols (96.8% sel.) with oxygen molecule as an ideal oxidant under mild conditions. Also, the nanohybrid showed an outstanding adsorption capability for benzyl alcohol (773 mg g^{-1}). In comparison to individual exfoliated V_2O_5 nanosheets and bulk V_2O_5, the V_2O_5-Al_{13} nanohybrid catalyst exhibited superior catalytic activity and selectivity under the same experiment condition. The result highlights the outstanding functionality of the V_2O_5-Al_{13} nanohybrid as an efficient oxidation catalyst. A detailed study of its structure-activity relationship showed that the high performance of V_2O_5-Al_{13} nanohybrid is attributed to the adsorption-catalytic synergistic effect between V_2O_5 and Al_{13}.

1. Introduction

The selective oxidation of alcohols to high-valued aldehydes and ketones represents one of the most significant organic transformation reactions in academic and industrial fields.[1-6] Over the past several years, a great deal of catalysts has been developed and used for catalytic oxidation of alcohols.[7-12] In particular, the supported noble metal nanoparticles (such as Au, Pd and Pt, et.al) are widely recognized to be one of the most efficient catalysts for liquid-phase oxidation of alcohols.[13-16] Although a great number of researches has been devoted to further improving the intrinsic catalytic activity of the precious metal catalysts, their high cost and low thermal stability have become a huge obstruct for their wide applications.[17-20] Therefore, exploring catalysts that are low cost, highly active and long-term stability under oxidizing conditions is very desirable.

Among many candidates as catalysts, vanadium oxides seem to be promising because of its natural abundance, low cost, excellent redox ability and good thermal stabilities.[21-23] Nevertheless, the real catalytic activity of vanadium oxides is largely dependent on crystal size, morphology and dimension, and a large number of researches have been devoted to synthesizing low-dimensional nanostructured vanadium oxides.[24-26] Of particular interest is the two-dimensional nanosheets of vanadium oxides prepared by exfoliation.[27] Compared with vanadium oxides nanospheres, two-dimensional vanadium oxides nanosheets with low agglomeration possess a larger surface area, and thus more active sites are exposed to improve catalytic performance.[28] However, it is well known that an excellent catalyst not only has an effective catalytic ability, but also shows a good adsorption effect on the substrate molecules.[29-31] Therefore, it is necessary to construct an adsorption-catalysis bifunctional hybrid material based on two-dimensional vanadium oxide nanosheets by introducing other functional guest molecules. Polyoxocations of Keggin-Al_{13} ($AlO_4Al_{12}(OH)_{24}(H_2O)_{12}^{7+}$) formed by the base hydrolysis of Al^{3+} aqueous solutions have been reported to show good adsorption capacity of organic pollutants.[32] Moreover, Keggin-Al_{13} polyoxocations have been widely used as a common pillaring agent for expanding the interlayer spacing of the host material.[33,34] Therefore, it is feasible to intercalate Keggin-Al_{13} into the interlayer of vanadium oxides nanosheets. Considering that Keggin-Al_{13} has a large amount of positive charges, it is expected to be more easily combined with negatively charged nanosheets, as a result, charged layered vanadium oxides nanosheets were prepared through soft chemical exfoliation.[35,36]

On the basis of the above considerations, we successfully prepared the first example of a porous nanohybrid based on electrostatic self-assembly of layered V_2O_5 and Keggin Al_{13} (V_2O_5-Al_{13}). The introduction of Keggin Al_{13} could effectively depress the aggregation of V_2O_5 nanosheets to expose more catalytically active sites as well as shorten diffusion path of organic molecules. The catalytic activity for oxidation of alcohols with as-prepared nanohybrid was tested and the results showed a high selectivity for producing aldehydes or ketones. In comparison with individual exfoliated V_2O_5 nanosheets and bulk V_2O_5, the nanohybrid had a significant improvement in catalytic activity, which is mainly attributed to the adsorption-catalysis synergistic effect of the V_2O_5-Al_{13} nanohybrid.

2. Experimental

---

[a] *Key Laboratory of Polyoxometalate Science of the Ministry of Education, College of Chemistry, Northeast Normal University, Jilin 130024, P. R. China.*

†Electronic Supplementary Information (ESI) available: [details of any supplementary information available should be included here]. See DOI: 10.1039/x0xx00000x

View Article Online
DOI: 10.1039/C9DT04485J

2.1 Chemicals

All chemicals were of analytical grade and were used as received without any further purification. V_2O_5, H_2O_2 (30%), NaOH, HCl, KCl and $AlCl_3{\cdot}6H_2O$ were purchased from Beijing Chemical Reagent. Tetrabutylamine hydroxide (TBAOH) was purchased from Aladdin Chemical Reagent. The various solvents such as 1,4-dioxane, acetonitrile and ethanol were obtained from Thomas Baker. The molecular oxygen used for catalytic reaction comes from air.

2.2 Sample preparation

2.2.1 Exfoliation of V_2O_5 nanosheets.

The $K_{0.42}V_2O_5{\cdot}0.25H_2O$ nanobelts were synthesized by chemical pre-intercalation approach that reported by Ekaterina Pomerantseva et al.[37] Typically, KCl was dissolved in 15 mL of deionized water and added to 15 mL of H_2O_2 (30wt%). Next, V_2O_5 powder was slowly added to the above solution under vigorous stirring. The molar ratio of K to V was kept at 10:1 to ensure excess of potassium in reaction mixture. After vigorous stirring for 1 h at room temperature, the mixture was then stirred for a further three hours at 60 °C. A powder with brown color was produced in solution and the mixture was aged for four days at room temperature. In the second step, the obtained aged sol (0.25 g) was dispersed in 15 mL of 3 M KCl aqueous solution. The mixture was placed in Teflon-lined steel autoclave and hydrothermally treated at 220 °C for 24 hours. The obtained $K_{0.42}V_2O_5{\cdot}0.25H_2O$ powder was filtered, washed with the deionized water and dried at 100 °C for 12 hours in air. A protonated form of $H_{0.42}V_2O_5{\cdot}0.3H_2O$ was synthesized by treating the $K_{0.42}V_2O_5{\cdot}0.25H_2O$ (~10 g) with HCl aqueous solution (1 dm^3, 1 mol dm^{-3}) under severely stirring for 10 days. The resulting sample (0.2 g) was then added into 200 cm^3 of TBAOH solution under stirring at room temperature for more than 2 weeks. The concentration of TBAOH ranged from 0.00213 mol dm^{-3} to 0.532 mol dm^{-3}. After the unexfoliated residue was separated by centrifugation at 11000 rpm, the resulting colloidal suspension containing well-dispersed exfoliated V_2O_5 nanosheets was obtained by freeze-dried.

2.2.2 Synthesis of Keggin Al_{13} ions.

A solution containing Al_{13} polyoxocations was prepared by dropwise addition of NaOH solution (100 cm^3, 0.48 mol dm^{-3}) to a $AlCl_3{\cdot}6H_2O$ solution (100 cm^3, 0.2 mol dm^{-3}) under stirring at 70 °C for 2 hours. The obtained solution was aged for overnight at room temperature.[38] The obtained OH/Al ratio of polyaluminum chloridemole solution (PAC) was 2.4. Subsequently, 30 ml of PAC solution was poured in a 500 mL conical flask and 300 mL of 1:5 ethanol-dioxane mixed solutions was slowly added under stirring for 2 hours. The obtained solution was aged for 2-4 hours and the white Keggin Al_{13} powders were produced.

2.2.3 Synthesis of V_2O_5-Al_{13} nanohybrid.

The nanohybrid was synthesized through mixing the aqueous solution of Keggin Al_{13} and layered V_2O_5 nanosheets under a constant stirring for 8 hours at room temperature. The resulting sample (abbreviated as V_2O_5-Al_{13}) was obtained by filtration, washed with absolute ethanol and then dried at 60 °C for 24 hours. The molar ratio of V_2O_5 nanosheets to Keggin Al_{13} was varied to tune the chemical components on the basis of charge balance (1:0.16).

2.3 Catalytic activity test.

Catalytic activities of the samples were evaluated by catalyzing oxidation of alcohols with molecular oxygen. For a typical run, benzyl alcohol (2.89 mmol), V_2O_5-Al_{13} catalyst (50 mg) and isobutyraldehyde (0.329 mmol) were added into the reactor containing acetonitrile (5 mL) under the magnetic stirring at 100 °C for 7 hours. The mixture was identified by GC-MS, and the product was analysed by GC with the internal standard using biphenyl as the internal standard.

2.4. Characterization.

Powder X-ray diffraction (PXRD) patterns were carried out using a Rigaku D/MAX-3 instrument with Cu *Kα* radiation in the angular range 2θ=5°-40° at 298 K. FT-IR spectra were recorded on an Alpha Centaurt spectrophotometer in the 400–4000 cm^{-1} range using KBr pellets. Scanning electron microscope (SEM) images and energy dispersive X-ray (EDX) analytical data were obtained by using a Quanta 250 FEG equipped with an EDX detector. Transmission electron microscope (TEM) images of V_2O_5 nanosheets and V_2O_5-Al_{13} nanohybrid were investigated by on a JEM -2100F operating at 200 kV. The HR-TEM images of V_2O_5 nanosheets and V_2O_5-Al_{13} nanohybrid were recorded on the JEM-2100F high-resolution transmission electron microscope. Surface morphology and elemental distribution of V_2O_5-Al_{13} nanohybrid were characterized with field emission-scanning electron microscopy. Organic components of the freeze-dried gel were recorded on an EA3000-type CHNS/O Elemental analyzer. Degree of proton exchange was evaluated through induced coupled plasma, or ICP spectrometry (LEEMAN-Prodigy). Thermogravimetric and differential thermal analyses (TG-DTA) were performed on a Rigaku TAS 200 thermal analyzer in flowing nitrogen at a heating rate of 10 °C min^{-1}. Raman spectra were recorded in backscattering geometry by exciting a sample on a slide glass with an Ar^+ laser of 488 nm (HR800). X-ray photoelectron spectroscopy (XPS) measurements were carried out at a Thermo ESCALAB 250Xray photoelectron spectrometer. Nitrogen adsorption-desorption isotherms were collected by an Autosorb volumetric gas sorption analyzer (ASAP 2020M) at -196 °C. The pore size distribution was calculated from the desorption branch of the isotherm based on the Barrett-Joyner-Halenda (BJH) method. Atomic force microscopy images (AFM) were performed using a Bruker Multimode 8 scanning probe microscope (Bruker Co. Ltd.).

View Article Online
DOI: 10.1039/C9DT04485J

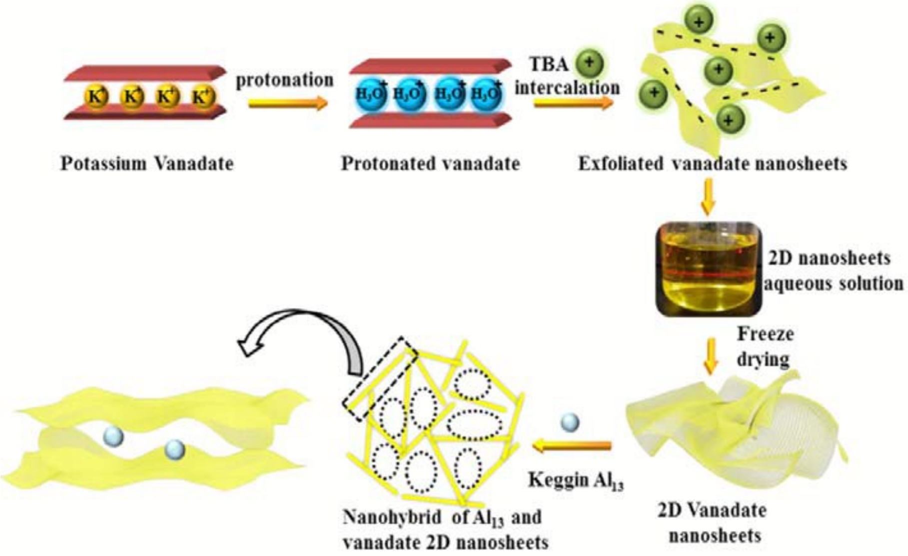

Scheme 1. Schematic diagram for the synthesis of nanohybrid of Keggin Al_{13} and 2D vanadate nanosheets.

3. Results and discussion

The single-phase layered vanadate $K_{0.42}V_2O_5{\cdot}0.25H_2O$ with high purity was confirmed via PXRD analysis. As is shown in Figure 1A-a, PXRD patterns of the sample exhibit characteristic diffraction peaks at 2θ of 9º and 27º corresponding to the (001) and (003) planes, respectively, which are very consistent with the reported data.[37] SEM imaging shows the layered vanadate $K_{0.42}V_2O_5{\cdot}0.25H_2O$ has a nanobelt morphology (Figure S1). To prepare protonated layered vanadate, K^+ ions in the interlayer were extracted by repeating the acid leaching. According to ICP analysis, the removal degrees of K^+ ions were 42.5%, 92.1% and 100% by reaction for 1, 3 and 10 days, respectively (Figure S2). Mean valence of vanadium in protonated layered vanadate was determined to be 4.79 by redox titration (Figure S3), which is the same as a mean valence of vanadium in $K_{0.42}V_2O_5{\cdot}0.25H_2O$. The water content was assessed through TGA over the temperature range of 100-500 °C and then the weight loss of the sample by calculation is approximately 2.85% corresponding to 0.3 water molecules in the protonated layered vanadate (Figure S4). Therefore, the composition of the protonated layered vanadate can be formulated as $H_{0.42}V_2O_5{\cdot}0.3H_2O$. Figure 1A-b shows the PXRD patterns of the obtained $H_{0.42}V_2O_5{\cdot}0.3H_2O$. According to the Bragg equation calculation, the interlayer spacing (d_{001}) of as-prepared $H_{0.42}V_2O_5{\cdot}0.3H_2O$ has enlarged to 11.2 Å compared with the 9.6 Å interlayer spacing (d_{001}) of $K_{0.42}V_2O_5{\cdot}0.25H_2O$, confirming the introduction of the larger ions in the interlayer space. Considering H^+ ions are mostly present in the form of H_3O^+ in water, as a consequence, the larger ions in interlayer of $H_{0.42}V_2O_5{\cdot}0.3H_2O$ are mainly H_3O^+.[39,40] FT-IR analysis (Figure 1B) further verified the formation of the protonated vanadate. Figure 1B-a represents the characteristic peaks of the fresh V_2O_5. Among them, the peaks at 1012 cm^{-1}, 748 cm^{-1} and 522 cm^{-1} are ascribed to the stretching vibration of V=O and V-O-V, respectively.[41] For $H_{0.42}V_2O_5{\cdot}0.3H_2O$, the FT-IR spectrum has obvious adsorption bands at 1630 cm^{-1} and 3400 cm^{-1}, which are attributed to the bending and stretching vibrations of H_3O^+ ions, respectively (Figure 1B-c and S5).[42] In addition, the peaks at 1012 cm^{-1} and 748 cm^{-1} occurred a significant blue shift compared to the fresh V_2O_5, suggesting that there is an interaction between the interlayer ions and the laminar V_2O_5 body (Figure 1B-b). SEM image shows that the as-prepared $H_{0.42}V_2O_5{\cdot}0.3H_2O$ is consists of micro-sheets with a high aspect ratio (Figure S6).

To further prepare layered vanadate nanosheets, the swelling and exfoliating behaviors of the obtained $H_{0.42}V_2O_5{\cdot}0.3H_2O$ were further investigated by treating with various concentrations of aqueous solution of tetrabutylammonium hydroxide (TBAOH). The molar ratio of TBA^+ ions to H^+ ions (abbreviated as TBA^+/H^+) in ions exchange process of $H_{0.42}V_2O_5{\cdot}0.3H_2O$ was ranged from 0.1 to 25. Among them, lots of visible solids were observed in the sample with a low TBA^+/H^+ (~0.1) by separation. In contrast, samples with $TBA^+/H^+ \geqq 1$ produced stable colloidal suspensions without noticeable sedimentation, which signifies the appearance of colloidal suspensions depending on the content of TBAOH. In order to investigate the degree of exfoliation of the $H_{0.42}V_2O_5{\cdot}0.3H_2O$ under different content of TBAOH in detail, the obtained colloidal suspension was centrifuged at high speed and then the upper liquid was freeze-dried to obtain exfoliated solid samples. It's worth noting that the volume and color of samples after treated with TBAOH (abbreviated as TBA-V_2O_5) have obvious changes compared to the protonated vanadate (Figure S8). The conspicuous increase of volume from the pristine $H_{0.42}V_2O_5{\cdot}0.3H_2O$ to TBA-V_2O_5 has been observed as the proportion of TBA^+/H^+ increases from 0.1 to 2, which clearly confirmed that the increment of TBAOH is beneficial to improve the interior space of the product. But what disappoints us is that the volume of TBA-V_2O_5 sample slightly decreased as the ratio of TBA^+/H^+ exceeds 2. This

View Article Online
DOI: 10.1039/C9DT04485J

phenomenon makes us suspect that the higher concentration of TBAOH does not support better exfoliation of V_2O_5. To test the conjecture, typical XRD patterns of these freeze-drying samples obtained at different ratio of TBA^+/H^+ were depicted in detail (Figure S9). A distinct sharp basal diffraction peak at about 7º was observed as the value of TBA^+/H^+ exceeds 5, and when the value of TBA^+/H^+ is equal to 25, the intensity of basal diffraction peak reaches the maximum. The Bragg peak corresponding to gallery height of the sample is 11.85 Å, which is only slightly larger than the origin value of 11.2 Å for the $H_{0.42}V_2O_5{\cdot}0.3H_2O$. Based on the previous study, we inferred that this expansion of the gallery height maybe due to the uptake of water into interlayer space and the pattern obtained above is ascribed to osmotic swelling.[43] In addition, a series of samples with $TBA^+/H^+ < 5$ were also analyzed. For $TBA^+/H^+ = 0.1$, the PXRD patterns of the sample showed that there are two immiscible phases, that is expanded (12.6 Å) and non-expanded (11.2 Å), simultaneously appeared. When the value of TBA^+/H^+ was further increased to 1, there is a sole phase in the freeze-drying sample. It is worth noting that when TBA^+/H^+ is equal to 2, a noticeable amorphous-like drum kit in a 2θ range of 5-10º was present (Figure 1A-c), which is ascribed to scattering from the agglomeration of exfoliated V_2O_5 sheets. On the basis of the above discussion, an important conclusion was educed, that is, a 2-fold excess to an equivalent amount of TBA ions (abbreviated as TBA-V_2O_5-2) to the exchangeable protons in $H_{0.42}V_2O_5{\cdot}0.3H_2O$ is the most optimized value for achieving complete delamination. The preparation process of the above material is illustrated in Scheme 1.

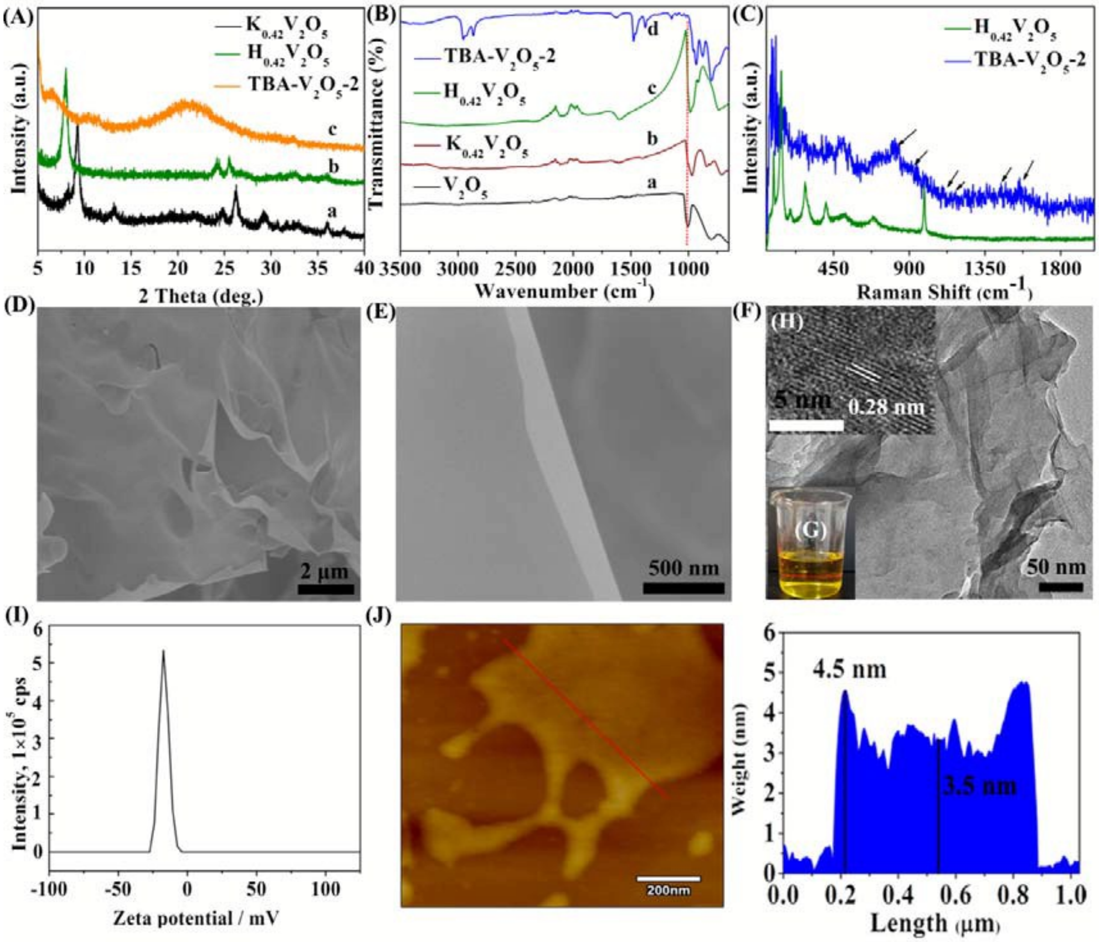

Figure 1. (A) Powder X-ray diffraction patterns of $K_{0.42}V_2O_5{\cdot}0.25H_2O$, $H_{0.42}V_2O_5{\cdot}0.3H_2O$ and TBA-V_2O_5-2 nanosheets, respectively. (B) FT-IR measurements of V_2O_5, $K_{0.42}V_2O_5{\cdot}0.25H_2O$, $H_{0.42}V_2O_5{\cdot}0.3H_2O$ and TBA-V_2O_5-2 nanosheets, respectively. (C) Raman spectra of $H_{0.42}V_2O_5{\cdot}0.3H_2O$ and TBA-V_2O_5-2 nanosheets, respectively. (D) SEM images of V_2O_5 nanosheets. (E) Edge curls view of the TBA-V_2O_5-2 nanosheets. (F) TEM images of TBA-V_2O_5-2 nanosheets. (G) Tyndall effect of TBA-V_2O_5-2 nanosheets. (H) HR-TEM images of TBA-V_2O_5-2 nanosheets. (I) Zeta potential curve of the colloidal suspension of exfoliated V_2O_5 nanosheets. (J) AFM image and corresponding height profiles of TBA-V_2O_5-2 nanosheets along the red line.

View Article Online
DOI: 10.1039/C9DT04485J

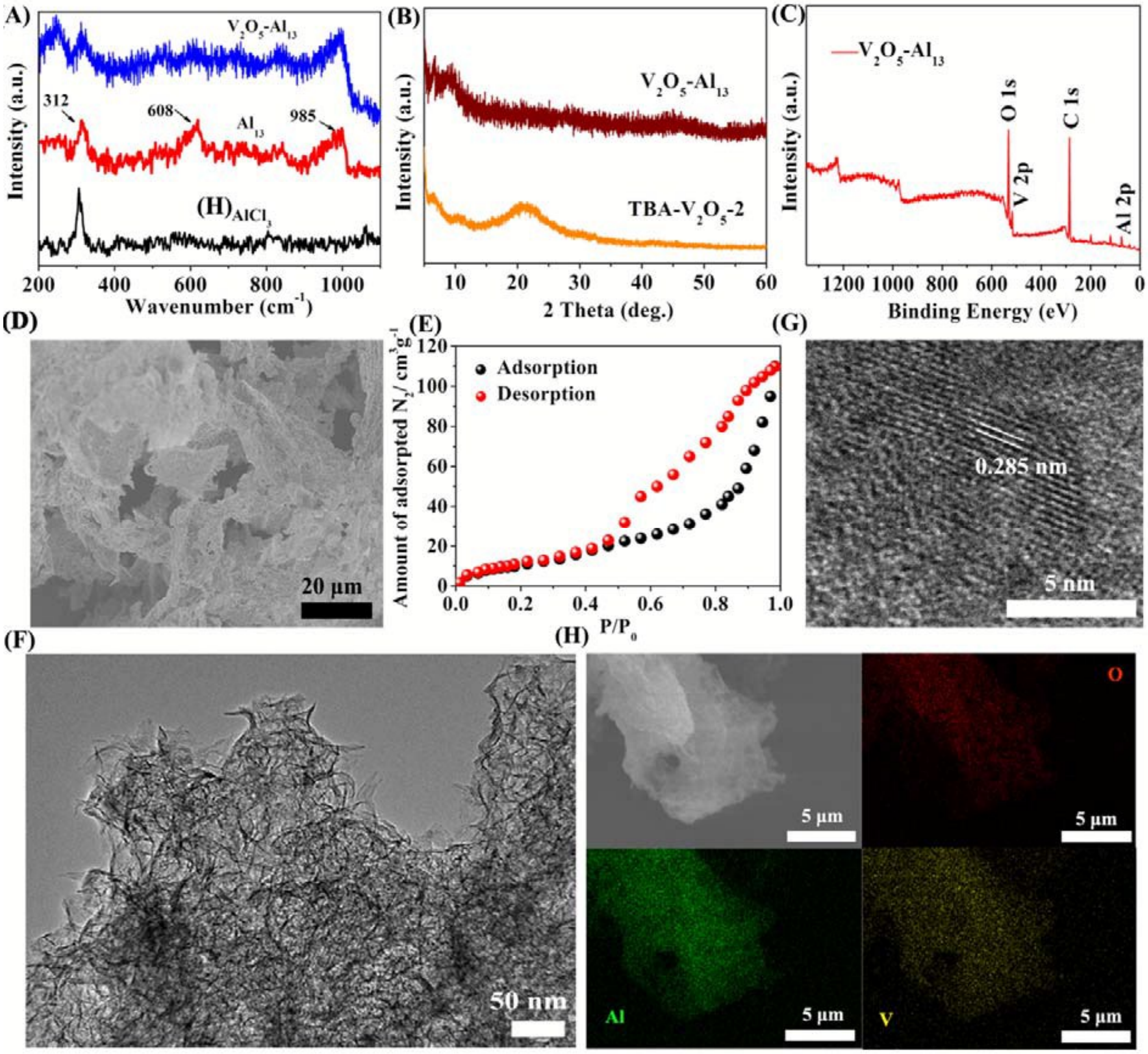

Figure 2. (A) Raman spectra measurements of Al_{13} salt, TBA-V_2O_5-2 nanosheets and V_2O_5-Al_{13} nanohybrid, respectively. (B) Powder X-ray diffraction patterns of Al_{13} salt, TBA-V_2O_5-2 nanosheets and V_2O_5- Al_{13} nanohybrid, respectively. (C) XPS full survey of V_2O_5-Al_{13} nanohybrid. (D) SEM images of V_2O_5- Al_{13} nanohybrid. (E) N_2 adsorption–desorption isotherms V_2O_5-Al_{13} nanohybrid. (F) HR-TEM images of a flaky aggregate. (G) Cross-sectional HR-TEM images for the as-prepared V_2O_5- Al_{13} nanohybrid (H) elemental mapping analysis of V_2O_5-Al_{13} nanohybrid .

The chemical composition of the TBA-V_2O_5-2 sample was further determined to be $(C_4H_9)_4N)_{0.67}H_{0.42}V_2O_5{\cdot}0.3H_2O$ through element analysis. Vibrational spectra in FT-IR (Figure 1B-d) also confirmed that the existence of TBA^+ ions and H_2O species simultaneously present in TBA-V_2O_5-2 sample. FT-IR peaks corresponding to 3336 and 1627 cm^{-1} are attributed to the stretching and bending vibration for H_2O, respectively. Sharp adsorptions in the range of 1000-1500 cm^{-1} and at 3000 cm^{-1} belong to the vibration of TBA^+ ions.[43] Raman spectrum (Figure 1C) shows the superposition of bands from TBA^+ and the V_2O_5 framework.[44] SEM picture shows that the TBA-V_2O_5-2 sample possesses thin enough and flexible nanosheets (Figure 1D and 1E). However, when the value of TBA^+/H^+ is less than 2, samples consist of a large number of agglomerated particles; and when the value of TBA^+/H^+ exceeds 5, these samples exhibited micron-thick layered structure; when the value of TBA^+/H^+ reached 25, a large number of stacked layers were obtained, demonstrating that high dose of TBA^+ ions would induce the production of osmotically swollen phase (Figure S10). TEM images of the TBA-V_2O_5-2 clearly showed exfoliated ultrathin nanosheets with curls or wrinkles (Figure 1F). The dispersion of TBA-V_2O_5-2 nanosheets was further confirmed by the light scattering experiment and a clear Tyndall effect was also observed clearly in upper bright yellow solution obtained by centrifugation (Figure 1G). Furthermore, close examination of the HR-TEM revealed a lattice spacing of 0.28 nm corresponding to the (301) plane of orthorhombic V_2O_5, which proved that the ultrathin TBA-V_2O_5-2 nanosheets still maintained high crystallinity (Figure 1H).[45] In addition, to deep

View Article Online
DOI: 10.1039/C9DT04485J

understand the oxidation state of the vanadium in the TBA-V_2O_5-2 nanosheets, XPS measurements were carried out and the spectra of V2p are shown in Figure S11. The peaks of both V2p3/2 and V2p1/2 were identified at 517.3, 516.1 eV and 524.5, 522.7 eV, corresponding to V^{4+} (516.1 and 522.7 eV) and V^{5+} (517.3 and 524.5 eV), respectively, confirming the presence of mixed-valence vanadium.[46] Meanwhile it is notable that the content ratio of V^{4+} peak and V^{5+} peak is about 1:2.5 by calculating the peak areas of V^{4+} and V^{5+}. It was because of the existence of V^{4+} that V_2O_5 nanosheets were negatively charged and the zeta potential measurement (Figure 1I) also demonstrates the electronegativity of the exfoliated V_2O_5 nanosheets. In order to further explore the synthesis of ultrathin nanosheets and understand their thickness, TBA-V_2O_5-2 nanosheets were examined by AFM and the results revealed that the thickness of most of the TBA-V_2O_5-2 nanosheets were approximately 3-5 nm (Figure 1J and Figure S12). The surface areas and pore structure of TBA-V_2O_5-2 nanosheets are examined with N_2 adsorption-desorption isotherm measurements. As is shown in Figure S13, the as-prepared V_2O_5 nanosheets possess smaller BET surface area of 36 m^2 g^{-1}, which may be due to the seriously restacking phenomenon between exfoliated nanosheets.

Table 1. Catalytic Performance of Different Catalysts for the Oxidation of Benzyl Alcohol to Benzaldehyde[a]

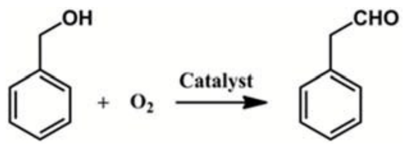

Catalysts	Time (h)	Conversion (%)	Selectivity (%)	Yield (%)
V_2O_5-Al_{13}	7	81.9	96.8	79.3
Al_{13}	7	5.4	0	0
Bulk V_2O_5	7	20.6	63	12.9
V_2O_5 nanosheets	7	32.9	67.5	22.2
VO(acac)$_2$	15	18.5	54.1	10
$VOCl_3$	16	24.9	69.2	17.2
No	12	-	-	-

[a] Reaction conditions: 2.89 mmol of benzyl alcohol. 50 mg of catalysts, 5 mL of acetonitrile, reaction temperature 100 °C, 1 atm O_2, 0.329 mmol of isobutyraldehyde. Conversion and yield were calculated on the basis of the formed product and consumed reactant as measured by GC-MS. Biphenyl was used as the internal standard

Based on the results shown above, TBA-V_2O_5-2 nanosheets were selected as the most suitable matrix to combine with Keggin Al_{13} polyoxocations. Among them, the V_2O_5-Al_{13} nanohybrid was synthesized based on the charge balance ratio of V_2O_5 nanosheets/ Keggin Al_{13} polyoxocations (V_2O_5 nanosheets: Al_{13} = 1:0.16). FT-IR spectra (Figure S14) of V_2O_5-Al_{13} nanohybrid display the characteristic peaks at 1625, 967, 818, 731, 546, and 457 cm^{-1}. Among them, the characteristic peaks of Keggin Al_{13} polyoxocations in nanohybrid changed significantly from 987 cm^{-1}, 1643 cm^{-1} to 967 cm^{-1} and 1625 cm^{-1}, respectively. Meanwhile, the characteristic asymmetric vibration of V-O-V shifts from 843 cm^{-1} in V_2O_5 nanosheets to 818 cm^{-1} for V_2O_5-Al_{13}, suggesting that a strong electrostatic interaction was presented between the exfoliated V_2O_5 nanosheets layers and the guest Al_{13} polyoxocations. As is shown in Figure 2A, Raman detection of the high purity Al_{13} salts shows three bands, that is a sharp one at 300 cm^{-1}, a broader one at 635 cm^{-1}, and a smaller one at 987 cm^{-1}, respectively. The above bands can be accordingly assigned to the vibrational modes of Al-OXs or the hydroxo group.[47-49] The Raman spectrum of V_2O_5-Al_{13} nanohybrid simultaneously shows characteristic signal peaks of Al_{13} polyoxocations and V_2O_5 nanosheets, which confirmed the successful combination of the two materials. It is a remarkable fact that these Raman peaks are not too strong, which may be due to their high signal-to-noise ratios. Figure 2B presents the PXRD patterns of the as-prepared V_2O_5-Al_{13} nanohybrid. In comparison with that of the TBA-V_2O_5-2 nanosheets, a broad diffraction envelope at 20° disappeared in V_2O_5-Al_{13} nanohybrid, which can be attributed to the combination of V_2O_5 nanosheets with Al_{13} polyoxocations. Furthermore, two diffraction peaks at 6.58° and 9.12° were observed in V_2O_5-Al_{13} nanohybrid. In light of the Bragg equation calculation, the former possesses an expanded basal spacing of 1.34~1.51 nm. Considering that the crystallographic thickness of V_2O_5 nanosheet is 0.42 nm[50] and the diameter of Keggin Al_{13} is 0.86 nm,[51] thus the repeating distance of V_2O_5-Al_{13} should be 1.28 nm, which is lower than the experimental value. This stupendous difference demonstrated that the layer-by-layer restacking structure was present in V_2O_5-Al_{13} nanohybrid. Since the V_2O_5 nanosheet has a negative charge of 1.09 to each chemical formula and one Al_{13} polyoxocation has a high positive charge of 7+, in other words, 7 unit cells of V_2O_5 nanosheets are required to balance the positive charge of one Al_{13} ion, Al_{13} ions were distributed sparsely in V_2O_5 nanosheets through electrostatic interactions. Of more importance, sparsely distributed Al_{13} polyoxocations could act as the inorganic linker to stabilize the multilayer assembly according to previous report,[33] therefore we inferred that the stacked V_2O_5 nanosheets can be opened through Al_{13} polyoxocations, which effectively increases the stacking space of the sheets and produces corresponding holes. From the second diffraction peak of 9.12°, a layer spacing can be calculated about 9.68 Å, which is lower than the sum of the thickness of two components, suggesting that Al_{13} polyoxocations and V_2O_5 nanosheets are assembled in other

View Article Online
DOI: 10.1039/C9DT04485J

Table 2. Selective Oxidation of Various Alcohols with V_2O_5-Al_{13} nanohybrid[a]

Entry	Substrate	Product	Conversion (%)	Selectivity (%)	Yield (%)
1	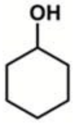	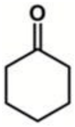	72.5	100	72.5
2	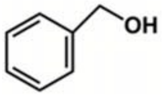	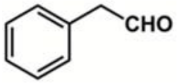	81.9	96.8	79.3
3	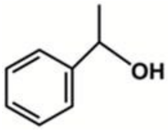	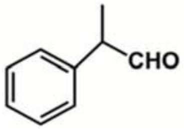	71.5	90.0	64.5
4	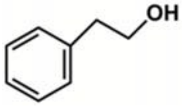	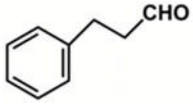	72.4	90.5	65.5
5		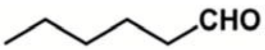	62.6	100	62.6
6			63.5	100	63.5
7	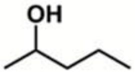	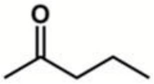	61.2	100	61.2
8	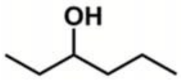	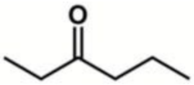	62.4	96	59.9

[a]Reaction conditions: 2.89 mmol of alcohols. 50 mg of catalysts, 5 mL of acetonitrile, reaction temperature 100 °C, reaction time 7 h, 1 atm O_2, 0.329 mmol of isobutyraldehyde. Conversion and yield were calculated on the basis of the formed product and consumed reactant as measured by gas chromatography. Biphenyl was used as the internal standard

forms other than the layer-by-layer mode. The reason for this behavior may be due to the relative lower charge of V_2O_5 nanosheets cannot accommodate Keggin Al_{13} polyoxocations in high packing density so that Keggin Al_{13} polyoxocations would not be completely inserted into the layer of V_2O_5 nanosheets.[52] XPS analysis was performed to further validate the elemental composition in V_2O_5-Al_{13} nanohybrid. As is shown in Figure 2C, the O 1s, V 2p and Al 2p signals are observed from the full survey. SEM images of the V_2O_5-Al_{13} nanohybrid show that there are porous structures by slice stacking in the as-prepared nanohybrid (Figure 2D). N_2 sorption isotherms (Figure 2E) of synthesized V_2O_5-Al_{13} nanohybrid exhibit weak adsorption of N_2 molecules in a low relative pressure region and a distinct hysteresis in the region of $p/p_0 > 0.5$ reveals that most of porosity in the present nanohybrid originates from mesoporous. Meanwhile, pore size analysis showed that the as-prepared V_2O_5-Al_{13} nanohybrid has an average diameter of 56 Å (Figure S15). TEM (Figure 2F) confirms that the as-prepared V_2O_5-Al_{13} nanohybrid still maintain the sheet morphology. Moreover, the formation of V_2O_5-Al_{13} nanohybrid structure is approved through the cross-sectional HR-TEM analysis. As illustrated in Figure 2G, a cross-sectional view of the as-prepared V_2O_5-Al_{13} nanohybrid shows an assembly of well-developed parallel dark stripes, which is attributed to layered V_2O_5 lattice. To further verify the hybridization between V_2O_5 nanosheets and Keggin Al_{13}, the spatial distributions of oxygen, vanadium and aluminum elements are evidenced with EDX (Figure S16) and elemental mapping analysis. As is plotted in Figure 2H, all elements of V_2O_5-Al_{13} nanohybrid are well distributed in nanohybrid, implying that two components are homogeneous mixed.

The catalytic performance of as-prepared V_2O_5-Al_{13} nanohybrid has been examined with respect to the selective oxidation of alcohols using molecule oxygen as a clean oxidant

View Article Online
DOI: 10.1039/C9DT04485J

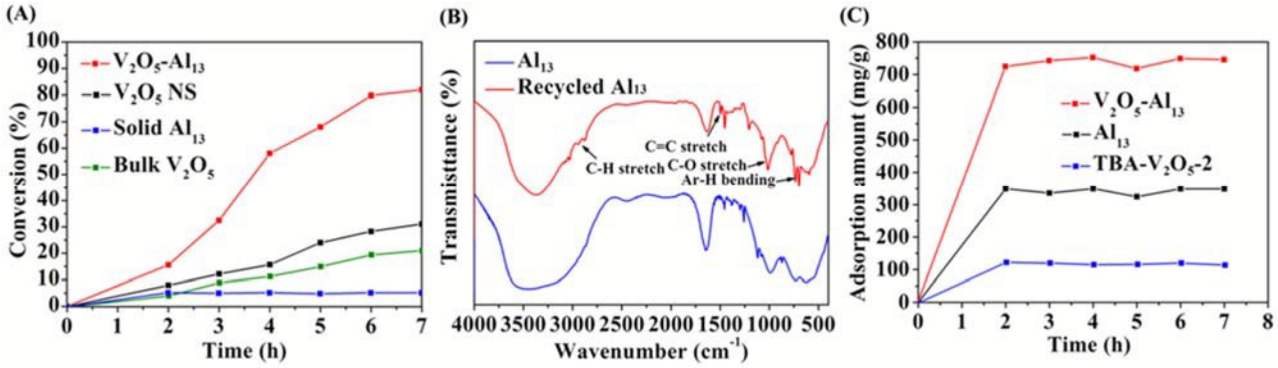

Figure 3. (A) Time profiles of catalytic oxidation of benzyl alcohol using different catalysts. (B) FT-IR spectra of single Al_{13} and benzyl alcohol-adsorbed on Al_{13}. (C) The amount of benzyl alcohol adsorbed by V_2O_5-Al_{13}, single solid Al_{13} and pure V_2O_5 nanosheets.

in presence of isobutyraldehyde. Among them, benzyl alcohol as a model substrate was catalyzed in a series of solvents. According to a large number of literature reports, acetonitrile, toluene, THF and ethanol are the most commonly organic solvents used to selective catalytic oxidation of alcohols. The experimental results showed that benzyl alcohol exhibited the best catalytic oxidation activity in acetonitrile (Table S1). This is because that acetonitrile is a polar solvent with a very high dielectric constant and it may readily dissolve isobutyraldehyde along with the benzyl alcohol and increase the efficiency of the catalytic system. Also, highly polar solvents like acetonitrile may facilitate formation of active oxygen species and thereby enhance the catalytic activity. The blank test was performed in the absence of catalysts, during which no product was observed. Meanwhile, the catalytic experience in the absence of isobutyraldehyde was also explored and the result showed that not any product was detected, which manifested that isobutyraldehyde plays an essential role in the catalytic oxidation reaction. To clearly clarify the oxidant role of molecule oxygen, the N_2 and Ar-purged the oxidation of benzyl alcohol was used as control experiments and the results displayed that benzyl alcohol did not undergo any conversion (Figure S17). Therefore, we speculated that O_2 is actually a key substance for initiating the occurrence of oxidation. Table 1 lists the catalytic oxidation of benzyl alcohol by V_2O_5-Al_{13} and a series of related vanadium-based analogues. V_2O_5-Al_{13} exhibits the best catalytic oxidation performance with 81.9% conversion and 96.8% selectivity. Under identical experimental conditions, the catalytic activities of bulk V_2O_5 and the exfoliated V_2O_5 nanosheets are estimated and the result showed that the exfoliated V_2O_5 nanosheets have a higher catalytic performance than that of bulk V_2O_5, indirectly signifying that the exfoliated V_2O_5 nanosheets can expose more catalytically active sites. In addition, the catalytic performance of the exfoliated V_2O_5 nanosheets is still lower than that of V_2O_5-Al_{13} nanohybrid, which explained that the hybridization of V_2O_5 nanosheets and Keggin Al_{13} is beneficial for improving the catalytic performance. Furthermore, the kinetic behavior analyses of different catalysts were also investigated in detail. The results illustrated that the catalytic reaction rate of the V_2O_5-Al_{13} is obviously quicker than that of bulk V_2O_5 and exfoliated V_2O_5 nanosheets in the first 7 hours, confirming the notable positive effect of hybridization on the catalytic activity (Figure 3A). When the reaction time was further extended to 12 h, the change of catalytic reaction rate based on V_2O_5 analogs is not obvious. The benzyl alcohol conversion profile between 7 and 12 hours of V_2O_5-based analogs are shown in Figure S18. It can be seen that there is very little benzyl alcohol conversion between 7 and 12 hours. Therefore, the catalytic performance study of V_2O_5-based analogs for the first 7 hours was more meaningful.

To understand the role of each component in V_2O_5-Al_{13} nanohybrid, the catalytic performance of single Al_{13} was in detail explored. Table 1 showed that Keggin Al_{13} has a negligible catalytic activity, which suggested that the true catalytic active centers are V_2O_5 nanosheets. But it is now apparent that the amount of benzyl alcohol has a certain decrease. We suspected that the phenomenon may be due to the fact that benzyl alcohol was adsorbed on Keggin Al_{13} rather than being catalyzed. To confirm the above speculation, the solid Al_{13} after reaction was recovered and characterized by FT-IR spectrum. As is shown in Figure 3B, a significant absorption peak around 1010 cm^{-1} on the surface of recovered Keggin Al_{13} was observed, which is attributed to C-O vibrations. Meanwhile, the Ar-H and O-H stretching vibrations were appeared in 700, 750 and 3300 cm^{-1}, respectively. The above analysis stated that there is an interaction between Keggin Al_{13} and the benzyl alcohol molecule. Moreover, compared to that of Keggin Al_{13} before the reaction, the characteristic peaks of the recovered Keggin Al_{13} significantly occurred to red-shift. This phenomenon also indicated the presence of chemisorption between Keggin Al_{13} and benzyl alcohol. In order to more intuitively clarify the adsorption of benzyl alcohol by Keggin Al_{13}, the adsorption amount of benzyl alcohol by different catalysts was detected (Figure 3C). Among them, the adsorption capacity of benzyl alcohol by Keggin Al_{13} reached 353 mg/g. In contrast, that by V_2O_5 nanosheets is about 121 mg/g, which is only one third of that by single Al_{13}. What's even more surprising is that the adsorption value for benzyl alcohol by V_2O_5-Al_{13} nanohybrid is up to 773 mg/g. In comparison to the single component of nanohybrid, the high adsorption ability of V_2O_5-Al_{13} nanohybrid is not only related to the adsorption performance of Keggin Al_{13}, but also attributed to the porous structure of the nanohybrid. On the basis of

View Article Online
DOI: 10.1039/C9DT04485J

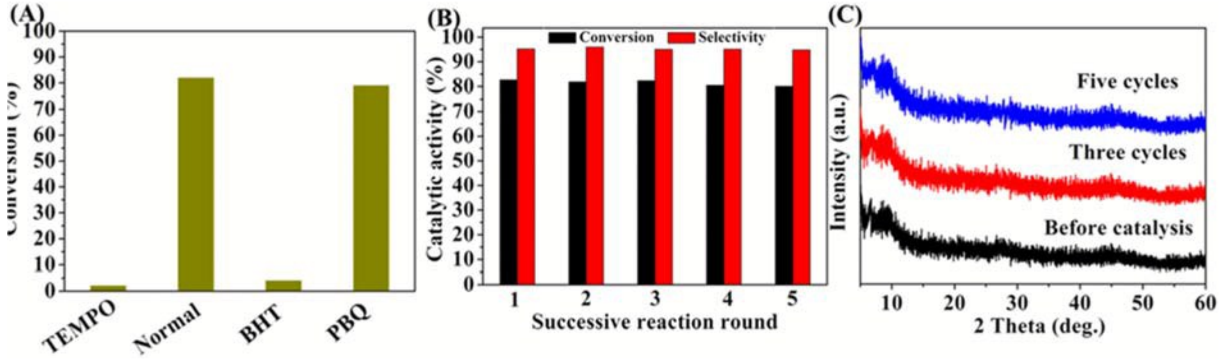

Figure 4. (A) Benzyl alcohol conversion over V_2O_5-Al_{13} nanohybrid in the presence of the different trapping species. (B) Recyclability of V_2O_5-Al_{13} nanohybrid in aerobic oxidation of alcohols. (C) PXRD patterns of V_2O_5-Al_{13} nanohybrid after recycling 5 times.

above analysis, we inferred that the high catalytic performance is attributed to synergistic effect of adsorption-catalysis between the exfoliated V_2O_5 nanosheets and Keggin Al_{13}.

Owing to V_2O_5-Al_{13} nanohybrid exhibiting the best catalytic activity among these catalysts, therefore we used it as the model catalyst to further evaluate the catalytic oxidation performance through extending the substrate scope. As is shown in Table 2, V_2O_5-Al_{13} nanohybrid can successfully induce a wide range of examples of selective alcohols oxidation. Among them, the yield of aliphatic alcohols exceeds 60%, significantly higher than those reported in the literature, where yields of < 44% were only able to be achieved for the selective oxidation of 1-heptanol using a V_2O_5 catalyst in the presence of base at 100 °C.[53] Using the as-prepared nanohybrid described here, the conversion rates of aromatic alcohols are excellent and the selectivity is up to 100% for the desired products. Such selectivity and efficacy are far superior to those reported previously in the literature using other V_2O_5-based catalysts (Table S2).[54-58]

To in-depth explore the reason for high selectivity of the V_2O_5-Al_{13} nanohybrid for oxidation of alcohols, the catalytic mechanism was investigated in detail. According to the previous reports, the oxidation pathway of alcohols generally was divided into two types, one is free radical path and another is non-radical path.[59] In order to test possible reaction pathway of this system, hydroquinone as an efficient radical scavenger was added to the catalytic system. The results showed that not any product peaks were detected by GC, thus we deduced that the catalytic reaction followed the free radical reaction path. Subsequently, to further define possible free-radicals produced in this system, we tried to add a series of reasonable free-radical scavengers to the reaction solution under the standard conditions. Among them, considering that isobutyraldehyde as a common sacrificial reagent usually could react with high valent metal centers to generate acyl radicals, which can act as a radical initiator to promote rapid process of reaction.[60] Hence we choose to add 2,2,6,6-tetramethylpiperidine-1-oxyl (TEMPO) as an efficient carbon radical scavenger to the catalytic system (Figure 4A).[61] The experimental results showed that the reaction basically has no conversions after 11 h of reaction, which strongly demonstrated the involvement of carbon-centered radical species in the present catalytic system, at the same time the GC test results showed the presence of isobutyricacid. Combining previously reported findings, we speculated the carbon-centered radical was the acyl free radical. Since oxygen molecule alone has not ability to oxidize alcohols, therefore we inferred that there may be other reactive oxygen species to oxidize alcohols in the system. To confirm this point of view, Ph_2NH as an oxygen-radical scavenger was added to catalytic system and an obvious inhibitory effect was observed, suggesting that oxygen active radicals are generated in this system.[62] In order to more clearly validate which oxygen active radicals actually exist in the system, we add 1,4-benzoquinone (PBQ) and 2,6-di-tert-butyl-4-methylphenol (BHT) to the catalytic system to specifically inhibit the generation of superoxide free radical and peroxyl free radical. As is shown in Figure 4A, only BHT could obviously suppress the oxidation of alcohols, which revealed that peroxyl free radical is the main oxygen active species. Summing up the previous reports, the generation of peroxyl free radical is inferred from the combination of acyl free radical with molecular oxygen. The generated peroxyl free radical typically combine with hydrogen ions to form isobutyric acid for oxidizing lots of organic substrates, including cycloolefins, alcohols and sulfides.[63, 64]

In view of the above exploration results, we have proposed a possible reaction pathway for oxidation of alcohols over the V_2O_5-Al_{13} nanohybrid catalyst. Here, it can undergo redox reaction with V^V centers in the nanohybrid catalyst to generate a large amount of acyl radicals, at the same time V^V centers would be reduced to V^{IV} centers. Subsequently, the produced acyl radicals react with molecular oxygen to afford the peroxy free radical. The unstable peroxy free radical could quickly abstract hydrogen from the aldehyde to give peroyacid. The obtained peroxyacid could oxidize adsorbed alcohol molecules on the one hand, and on the other hand they would react with V^{IV} centers to give high-valent vanadium centers so as to keep the catalyst structure unchanged.

In the final set of experiments, the reusability of the V_2O_5-Al_{13} catalyst was investigated because it is important to signify that the highly active catalyst is stable under oxidizing conditions. After five catalytic cycles, the nanohybrid was recycled from the reaction mixture by centrifugation. Catalytic

View Article Online
DOI: 10.1039/C9DT04485J

results revealed that no clear loss of activity was observed in five runs (Figure 4B). PXRD characterization showed that the structure of catalyst was mostly retained (Figure 4C). ICP measurements indicated that only traces of metal (< 1% of the total vanadium or aluminum) were detected. SEM image of V_2O_5-Al_{13} nanohybrid after five catalytic runs was shown in Figure S19, which revealed a certain degree of aggregation through drying. The HR-TEM image also indicated that the hybrid material after catalysis still showed the shape of the sheet stack (Figure S20). The above results commonly confirmed that the V_2O_5-Al_{13} nanohybrid was a stable and highly efficient catalyst for aerobic oxidation of alcohols.

Conclusion

In summary, a porous V_2O_5-Al_{13} nanohybrid was for the first time synthesized through electrostatic self-assembly between positively charged Keggin Al_{13} and negatively charged exfoliated V_2O_5 nanosheets for selective catalytic oxidation of alcohols under oxygen atmosphere. The experiment results exhibited that the V_2O_5-Al_{13} nanohybrid has a marked superiority (86.2% con.) over catalytic activity than bulk V_2O_5 and exfoliated V_2O_5 nanosheets, which is attributed to a synergistic coupling of adsorption-catalysis between the V_2O_5 nanosheets and Keggin Al_{13}. Moreover, the V_2O_5-Al_{13} naohybrid maintained a high conversion and selectivity during five recycles and the recycled catalyst still has a high stability. The combination of highly catalytic performance and high stability enables the V_2O_5-Al_{13} nanohybrid as an excellent catalyst for replacing previously expensive metals-based catalyst.

Conflicts of interest

There are no conflicts to declare.

Acknowledgements

We are grateful to the reviewers for their insightful comments and valuable suggestions. This work was financially supported by the National Natural Science Foundation of China (Grant Nos. 21571030)

Notes and references

1 B. Karimi, M. Khorasani, H. Vali, C. Vargas and R. Luque, *ACS Catalysis*, 2015, **5**, 4189-4200.
2 M. Mohammadi, A. Rezaei, A. Khazaei, S. Xuwei and Z. Huajun, *ACS Appl. Mater. Interfaces*, 2019, **11**, 33194-33206.
3 R. A. Sheldon, I. W. C. E. Arends, G.-J. ten Brink and A. Dijksman, *Accounts Chem. Res.*, 2002, **35**, 774-781.
4 D. I. Enache, J. K. Edwards, P. Landon, B. Solsona-Espriu, A. F. Carley, A. A. Herzing, M. Watanabe, C. J. Kiely, D. W. Knight and G. J. Hutchings, *Science*, 2006, **311**, 362.
5 A. Abad, P. Concepcion, A. Corma and H. Garcia, *Angew. Chem. Int. Ed.*, 2005, **44**, 4066-4069.
6 T. Mallat and A. Baiker, *Chem. Rev.,* 2004, **104**, 3037-3058.
7 F. Ferretti, A. P. C. Ribeiro, E. Alegria, A. M. Ferraria, M. N. Kopylovich, M. F. C. Guedes da Silva, F. Marchetti and A. J. L. Pombeiro, *Dalton Trans.*, 2019, **48**, 3198-3203.
8 Z. Wei, S. Ru, Q. Zhao, H. Yu, G. Zhang and Y. Wei, *Green Chem.*, 2019, **21**, 4069-4075.
9 C. Xiao, L. Zhang, H. Hao and W. Wang, *ACS Sustain. Chem. Eng.*, 2019, **7**, 7268-7276.
10 Z. Wei, S. Ru, Q. Zhao, H. Yu, G. Zhang and Y. Wei, *Green Chem.*, 2019, **21**, 4069-4075.
11 P. Guo, Q. Fu, C. Yildiz, Y.-T. Chen, K. Ollegott, C. Froese, W. Kleist, R. A. Fischer, Y. Wang, M. Muhler and B. Peng, *Catal. Sci. Technol.*, 2019, **9**, 3703-3710.
12 Z. Guo, B. Liu, Q. Zhang, W. Deng, Y. Wang and Y. Yang, *Chem. Soc. Rev.,* 2014, **43**, 3480-3524.
13 H. Li, F. Qin, Z. Yang, X. Cui, J. Wang and L. Zhang, *J. Am. Chem. Soc.*, 2017, **139**, 3513-3521.
14 R. Long, K. Mao, X. Ye, W. Yan, Y. Huang, J. Wang, Y. Fu, X. Wang, X. Wu, Y. Xie and Y. Xiong, *J. Am. Chem. Soc.*, 2013, **135**, 3200-3207.
15 Y. Z. Chen, Z. U. Wang, H. Wang, J. Lu, S. H. Yu and H. L. Jiang, *J. Am. Chem. Soc.*, 2017, **139**, 2035-2044.
16 Z. Tang, D. G. Boer, A. Syariati, M. Enache, P. Rudolf, H. J. Heeres and P. P. Pescarmona, *Green Chem.*, 2019, **21**, 4115-4126.
17 Y. Du, Q. Wang, X. Liang, Y. He, J. Feng and D. Li, *J. Catal.*, 2015, **331**, 154-161.
18 P. C. K. Vesborg and T. F. Jaramillo, *RSC Adv.*, 2012, **2**, 7933.
19 L.-B. Lv, S.-Z. Yang, W.-Y. Ke, H.-H. Wang, B. Zhang, P. Zhang, X.-H. Li, M. F. Chisholm and J.-S. Chen, *ChemCatChem*, 2018, **10**, 3539-3545.
20 H. Su, K. X. Zhang, B. Zhang, H. H. Wang, Q. Y. Yu, X. H. Li, M. Antonietti and J. S. Chen, *J. Am. Chem. Soc.*, 2017, **139**, 811-818.
21 S. Zavahir, Q. Xiao, S. Sarina, J. Zhao, S. Bottle, M. Wellard, J. Jia, L. Jing, Y. Huang, J. P. Blinco, H. Wu and H.-Y. Zhu, *ACS Catalysis*, 2016, **6**, 3580-3588.
22 Y. Zhang, Y. Qi, Z. Yin, H. Wang, B. He, X. Liang, J. Li and Z. Li, *Green Chem.*, 2018, **20**, 3944-3953.
23 H. Zou, G. Xiao, K. Chen and X. Peng, *Dalton Trans.*, 2018, **47**, 13565-13572.
24 M. Fattahi, M. Kazemeini, F. Khorasheh and A. M. Rashidi, *Catal. Sci. Technol.*, 2015, **5**, 910-924.
25 M. Pradhan, A. Roy, A. K. Sinha, R. Sahoo, D. Deb and T. Pal, *Dalton Trans.*, 2015, **44**, 1889-1899.
26 E. Uchaker, N. Zhou, Y. Li and G. Cao, *J. Phys. Chem. C*, 2013, **117**, 1621-1626.
27 R. Cai, J. Chen, D. Yang, Z. Zhang, S. Peng, J. Wu, W. Zhang, C. Zhu, T. M. Lim, H. Zhang and Q. Yan, *ACS Appl. Mater. Interfaces*, 2013, **5**, 10389-10394.
28 Y. Qi, K. Qin, Z. Jian, X. Yang, W. Jin, Y. Tan, Y. Zou and W. Chen, *J. Mater. Sci.*, 2019, **54**, 12713-12722.
29 Y. Liu, S. Liu, S. Liu, D. Liang, S. Li, Q. Tang, X. Wang, J. Miao, Z. Shi and Z. Zheng, *ChemCatChem*, 2013, **5**, 3086-3091.
30 B. Yang, R. Burch, C. Hardacre, G. Headdock and P. Hu, *ACS Catalysis*, 2013, **4**, 182-186.
31 M. Almasi, V. Zelenak, R. Gyepes, S. Bourrelly, M. V. Opanasenko, P. L. Llewellyn and J. Cejka, *Inorg. Chem.*, 2018, **57**, 1774-1786.
32 W. H. Casey, *Chem. Rev*, 2006, **106**, 1-16.
33 Wang, N. Sakai, Y. Ebina, K. Takada and T. Sasaki, *Chem. Mater.*, 2005, **17**, 1352-1357.
34 K. Wen, J. Zhu, H. Chen, L. Ma, H. Liu, R. Zhu, Y. Xi and H. He, *Langmuir*, 2019, **35**, 382-390.
35 J. L. Gunjakar, I. Y. Kim, J. M. Lee, Y. K. Jo and S.-J. Hwang, *J. Phys. Chem. C.*, 2014, **118**, 3847-3863.
36 Y. Chen, Z. Yao, H. N. Miras and Y. F. Song, *Chemistry*, 2015, **21**, 10812-10820.

View Article Online
DOI: 10.1039/C9DT04485J

37 M. Clites, J. L. Hart, M. L. Taheri and E. Pomerantseva, *ACS Energy Lett.*, 2018, **3**, 562-567.
38 F. Kooli, T. Sasaki and M. Watanabe, *Chem. Commun.*, 1999, 211-212.
39 J. M. Lee, B. Kang, Y. K. Jo and S. J. Hwang, *ACS Appl. Mater. Interfaces*, 2019, **11**, 12121-12132.
40 W. Chen, J. Peng, L. Mai, Q. Zhu and Q. Xu, *Mater. Lett.*, 2004, **58**, 2275-2278.
41 C. V. Subba Reddy, S.-i. Mho, R. R. Kalluru and Q. L. Williams, *J. Power. Sources*, 2008, **179**, 854-857.
42 Q. Wei, J. Liu, W. Feng, J. Sheng, X. Tian, L. He, Q. An and L. Mai, *J. Mater. Chem. A*, 2015, **3**, 8070-8075.
43 T. Sasaki and M. Watanabe, *J. Am. Chem. Soc.*, 1998, **120**, 4682-4689.
44 T. Sasaki, S. Nakano, S. Yamauchi and M. Watanabe, *Chem. Mater.*, 1997, **9**, 602-608.
45 X. Rui, Z. Lu, H. Yu, D. Yang, H. H. Hng, T. M. Lim and Q. Yan, *Nanoscale*, 2013, **5**, 556-560.
46 S. Zavahir, Q. Xiao, S. Sarina, J. Zhao, S. Bottle, M. Wellard, J. Jia, L. Jing, Y. Huang, J. P. Blinco, H. Wu and H.-Y. Zhu, *ACS Catalysis*, 2016, **6**, 3580-3588.
47 N. Li, C. Hu, X. Fu, X. Xu, R. Liu, H. Liu and J. Qu, *Environ. Sci. Technol.*, 2017, **51**, 2899-2906.
48 C. C. Alves, T. B. C. Campos and W. A. Alves, *Spectrochimica Acta Part A: Molecular and Biomolecular Spectroscopy*, 2012, **97**, 1085-1088.
49 H. G. M. Edwards, D. W. Farwell and A. F. Johnson, *J. Mol. Struct.*, 1995, **344**, 37-44.
50 A. B. Ganganboina, A. Dutta Chowdhury and R. A. Doong, *ACS Appl. Mater. Interfaces*, 2018, **10**, 614-624.
51 K. Ohtsuka, *Chem. Mater.*, 1997, **9**, 2039-2050.
52 Wang, Y. Ebina, K. Takada and T. Sasaki, *J. Phys. Chem. B*, 2004, **108**, 4283-4288.
53 S. Velusamy and T. Punniyamurthy, *Org. Lett.*, 2004, **6**, 217-219.
54 N. Anbu, M. B. Ruby Kamalam, K. Sethuraman and A. Dhakshinamoorthy, *ChemistrySelect*, 2018, **3**, 12725-12733.
55 V. Mahdavi and S. Soleimani, *Mater. Res. Bull.*, 2014, **51**, 153-160.
56 P. S. N. Rao, K. T. V. Rao, P. S. S. A. I. Prasad and N. Lingaiah, *Chin. J. Catal.*, 2011, **32**, 1719-1726.
57 P. S. N. Rao, A. Srihari Kumar, P. S. Sai Prasad and N. Lingaiah, *Reaction Kinetics, Mechanisms and Catalysis*, 2011, **105**, 429-440.
58 P. Renu, T. Radhika and S. Sugunan, *Catal. Commun.*, 2008, **9**, 584-589.
59 S. Murahashi, T. Naota and N. Hirai, *J. Org. Chem.*, 1993, **58**, 7318-7319.
60 B. B. Wentzel, P. L. Alsters, M. C. Feiters and R. J. M. Nolte, *J. Org. Chem.*, 2004, **69**, 3453-3464.
61 Q.-T. He, X.-P. Li, L.-F. Chen, L. Zhang, W. Wang and C.-Y. Su, *ACS Catalysis*, 2013, **3**, 1-9.
62 J.-K. Li, X.-Q. Huang, S. Yang, H.-W. Ma, Y.-N. Chi and C.-W. Hu, *Inorg. Chem.*, 2015, **54**, 1454-1461.
63 A. M. Khenkin, A. Rosenberger and R. Neumann, *J. Catal.*, 1999, **182**, 82-91.
64 S. Wang, Y. Liu, Z. Zhang, X. Li, H. Tian, T. Yan, X. Zhang, S. Liu, X. Sun, L. Xu, F. Luo and S. Liu, *ACS Appl. Mater. Interfaces*, 2019, **11**, 12786-12796.

Table of Contents

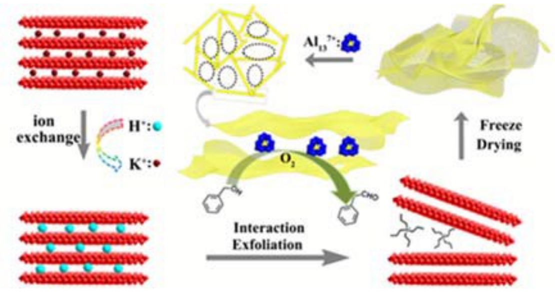

A porous V_2O_5-Al_{13} nanohybrid based on self-assembly of Keggin Al_{13} and exfoliated V_2O_5 nanosheets for selective oxidation of alcohols.